# Pion production in a transport model based on mean fields from chiral effective field theory

Zhen Zhang*
*Cyclotron Institute and Department of Physics and Astronomy, Texas A&M University, College Station, Texas 77843, USA*

Che Ming Ko†
*Cyclotron Institute and Department of Physics and Astronomy, Texas A&M University, College Station, Texas 77843, USA*

(Received 27 August 2018; published 26 November 2018)

We develop a Boltzmann-Uehling-Uhlenbeck (BUU) transport model based on the Sk$\chi$m$^*$ energy density functional, which is constructed from fitting the nuclear equation of state and nucleon effective masses in asymmetric nuclear matter predicted by the two- and three-body chiral interactions as well as the binding energies of finite nuclei. This new $\chi$BUU transport model is then used to study how baryon mean-field potentials affect the kinematics of a scattering or decay process and the equilibrium properties of a hot $N$-$\Delta$-$\pi$ system in a box with periodic boundary conditions. We find that the inclusion of mean-field potentials in the energy conservation condition for scattering and decay processes is necessary to maintain the equilibrium numbers of $N$, $\Delta$, and $\pi$. Although the baryon mean-field potentials have significant effects on the total $\Delta$ and $\pi$ numbers, they only slightly affect the ratio of effective negatively to positively charged pions. We also study pion production in central $^{197}$Au + $^{197}$Au collisions at the incident energy of $E/A = 400$ MeV and compare the results with the experimental data from the Four Pi (FOPI) Collaboration at the Gesellschaft für Schwerionenforschung mbH (GSI) in Germany. We find that our model can well describe the experimental results and the threshold effect due to baryon mean-field potentials does not affect much the charged pion ratio in this model. We further make predictions on pion production for the ongoing experiments of $^{132}$Sn + $^{124}$Sn and $^{108}$Sn + $^{112}$Sn at the incident energy of $E/A = 270$ MeV by the SAMURAI Pion-Reconstruction and Ion-Tracker (S$\pi$RIT) Collaboration at the Institute of Physical and Chemical Research (RIKEN) in Japan.

DOI: 10.1103/PhysRevC.98.054614

## I. INTRODUCTION

Chiral effective field theory provides a systematic framework for constructing the nucleon-nucleon interactions based on the symmetries of QCD and their breakings [1,2]. The resulting chiral nuclear interactions have been extensively used in various many-body methods, such as the no-core shell model [3], quantum Monte Carlo methods [4], coupled-cluster method [5], and in-medium similarity renormalizaton group theory [6] to study properties of light- and medium-mass nuclei as well as infinite nuclear matter. Although significant progress has been achieved in these *ab initio* calculations, it is still a challenge to use chiral nuclear interactions for studying more complicated nuclear systems, such as heavy nuclei and neutron stars. Also, there has not been any attempt to implement the chiral nuclear interactions in the transport model to study the dynamics of heavy-ion collisions. For these cases, the most feasible approach is to use the nuclear energy density functional constrained by chiral effective field theory [7–9]. Very recently, a new Skyrme energy density functional, called Sk$\chi$m$^*$, has been constructed from fitting the equation of state of asymmetric nuclear matter and nucleon effective masses from chiral two- and three-body forces [10,11] as well as the binding energies of finite nuclei, and it has been successfully used in studying the nuclear giant dipole resonance [8]. In this work, we employ the Sk$\chi$m$^*$ energy density functional in a Boltzmann-Uehling-Uhlenbeck (BUU) transport model to study pion production in intermediate-energy heavy-ion collisions.

The study of pion production in heavy-ion collisions near the threshold energy has recently attracted much attention since the charged pion ratio from these collisions has been proposed as a unique probe of the high-density behavior of nuclear symmetry energy [12]. The latter is essential for understanding the properties of neutron stars and the gravitational waves from spiraling neutron star binary but is still poorly known [13–17]. During the past decade, a lot of effort has been devoted to studying and exploring the possibility of determining from pion production in heavy-ion collisions the properties of nuclear symmetry energy at high densities [18–32]. With soon to be available systematic experimental measurements of the pion yield from intermediate-energy heavy-ion collisions, which are being carried out by the SPiRIT Collaboration at RIKEN in Japan [33], theoretical studies of pion production become even more important.

Before employing the Sk$\chi$m$^*$ energy density functional to study pion production in heavy-ion collisions, we first

*Present address: Sino-French Institute of Nuclear Engineering and Technology, Sun Yat-Sen University, Zhuhai 519082, China; zhangzh275@mail.sysu.edu.cn
†ko@comp.tamu.edu

 

carry out a box calculation with periodic boundary conditions to investigate the effect of energy conservation in nucleon-$\Delta$ inelastic scattering, $\Delta$ decay, and pion absorption in the presence of mean-field potentials on the equilibrium properties of a hot $N$-$\Delta$-$\pi$ matter. We find that the inclusion of baryon mean-field potentials in the energy conservation condition is necessary to maintain the equilibrium numbers and momentum distributions of $N$, $\Delta$, and $\pi$. Without taking into this account, the $\Delta$ and $\pi$ equilibrium numbers would be significantly affected, although the charged pion ratio is only slightly modified. We then study pion production in central $^{197}$Au + $^{197}$Au collisions at the incident energy of $E/A =$ 400 MeV. As in the case of box calculations, including baryon mean-field potentials in the energy conservation condition in nucleon-$\Delta$ inelastic scattering, $\Delta$ decay, and pion absorption has a significant effect on the total pion yield but only slightly affects the charged pion ratio. By introducing a density dependence in the $\delta$ production cross section, our model can well reproduce the experimental data on both the total pion yield and the charged pion ratio. Finally, we make predictions on the double and subtracted charged pion ratio as well as the isoscaling pion yield ratio in midcentral $^{132}$Sn + $^{124}$Sn and $^{108}$Sn + $^{112}$Sn collisions at the incident energy of $E/A = 270$ MeV that are being studied in the ongoing experiment by the SPiRIT Collaboration.

This paper is organized as follows. In Sec. II, we give an introduction to our Boltzmann-Uehling-Uhlenbeck transport model including the baryon mean-field potentials, the scattering cross sections and the in-medium $\Delta$ decay width, and the detailed balance relations for the $NN \leftrightarrow N\Delta$ and $\Delta \leftrightarrow N\pi$ processes in medium. Results from box calculations and heavy-ion collisions using this transport model are shown in Sec. III. Finally, we give a summary in Sec. IV.

## II. THE BOLTZMANN-UEHLING-UHLENBECK MODEL

In the present work, the time evolution of the single-particle distribution functions $f_i(\boldsymbol{r}, \boldsymbol{p}; t)$, where $i$ denotes $N$, $\Delta$, and $\pi$ in various charge states, in phase space is described by the Boltzmann-Uehling-Uhlenbeck equation, which can be written as

$$\frac{\partial}{\partial t} f_i + \nabla_{\boldsymbol{p}} E_i \cdot \nabla_{\boldsymbol{r}} f_i - \nabla_{\boldsymbol{r}} E_i \cdot \nabla_{\boldsymbol{p}} f_i = \mathcal{C}. \tag{1}$$

In the above, $E_i$ is the single-particle energy and $\mathcal{C}$ denotes the collision integral, which includes baryon-baryon elastic scattering and inelastic scattering that produces or absorbs a $\Delta$ resonance, $\Delta$ decay, and $\pi$ absorption. Because of the nonrelativistic nature of Sk$\chi$m$^*$ interaction, we treat nucleons and $\Delta$ resonances as nonrelativistic particles with their single-particle energies given by $E_i = m_i + \frac{\mathbf{p}_i^2}{2m_i} + U_i$, where $m_i$, $\mathbf{p}_i$, and $U_i$ are the mass, momentum, and potential, respectively. For pions, they are treated as relativistic particles due to their small masses (138 MeV), and their single-particle energies are taken to be $E_\pi = \sqrt{m_\pi^2 + \mathbf{p}_\pi^2}$ by neglecting their potentials as in most transport models.

### A. Baryon mean-field potentials

We include only the mean-field potentials of baryons while we treat pions as if they are in free space. The potentials for nucleons and $\Delta$ resonances are taken from the nonrelativistic Sk$\chi$m$^*$ energy density functional, which is constructed from fitting the nuclear equation of state and nucleon effective masses from the chiral effective field theory and the binding energies of finite nuclei [8]. In uniform nuclear matter, the potential energy part of the Sk$\chi$m$^*$ energy density functional has the form [34]

$$\begin{aligned}\varepsilon_{\rm pot}(\boldsymbol{r}) = {} & A_0\rho^2 - A_1\left(\rho_n^2 + \rho_p^2\right) + B_0\rho^{\alpha+2} - B_1\rho^\alpha\left(\rho_n^2 + \rho_p^2\right) \\ & + C\int d^3\boldsymbol{p}d^3\boldsymbol{p}' f(\boldsymbol{r}, \boldsymbol{p}) f(\boldsymbol{r}, \boldsymbol{p}')(\boldsymbol{p} - \boldsymbol{p}')^2 \\ & + D\int d^3\boldsymbol{p}d^3\boldsymbol{p}'[f_n(\boldsymbol{r}, \boldsymbol{p}) f_n(\boldsymbol{r}, \boldsymbol{p}')(\boldsymbol{p} - \boldsymbol{p}')^2 \\ & + f_p(\boldsymbol{r}, \boldsymbol{p}) f_p(\boldsymbol{r}, \boldsymbol{p}')(\boldsymbol{p} - \boldsymbol{p}')^2], \end{aligned} \tag{2}$$

where $f = f_p + f_n$ with $f_p(f_n)$ being the phase-space distribution function of protons (neutrons) and $\rho(\mathbf{r}) = \rho_p(\mathbf{r}) + \rho_n(\boldsymbol{r})$ with $\rho_p(\boldsymbol{r}) = \int d^3\boldsymbol{p} f_p(\mathbf{r}, \boldsymbol{p})$ [$\rho_n(\boldsymbol{r}) = \int d^3\boldsymbol{p} f_n(\mathbf{r}, \boldsymbol{p})$] being the proton (neutron) density at $\boldsymbol{r}$. The coefficients $A_0$, $A_1$, $B_0$, $B_1$, $C$, and $D$ can be expressed in terms of the parameters in the conventional Skyrme interaction,

$$\begin{aligned} v(\boldsymbol{r}_1, \boldsymbol{r}_2) = {} & t_0(1 + x_0P_\sigma)\delta(\boldsymbol{r}_1 - \boldsymbol{r}_2) \\ & + \frac{1}{2}t_1(1 + x_1P_\sigma)[\boldsymbol{p}'^2\delta(\boldsymbol{r}_1 - \boldsymbol{r}_2) + \text{c.c.}] \\ & + t_2(1 + x_2P_\sigma)\boldsymbol{p}' \cdot \delta(\boldsymbol{r}_1 - \boldsymbol{r}_2)\boldsymbol{p} \\ & + \frac{1}{6}t_3(1 + x_3P_\sigma)\rho^\alpha\left(\frac{\boldsymbol{r}_1 + \boldsymbol{r}_2}{2}\right)\delta(\boldsymbol{r}_1 - \boldsymbol{r}_2) \\ & + iW_0(\boldsymbol{\sigma}_1 + \boldsymbol{\sigma}_2) \cdot [\boldsymbol{p}' \times \delta(\boldsymbol{r}_1 - \boldsymbol{r}_2)\boldsymbol{p}], \end{aligned} \tag{3}$$

where $\boldsymbol{\sigma}_i$ is the Pauli spin operator, $P_\sigma = (1 + \boldsymbol{\sigma}_1 \cdot \boldsymbol{\sigma}_2)/2$ is the spin-exchange operator, $\boldsymbol{p} = -i(\nabla_1 - \nabla_2)/2$ is the relative momentum operator, and $\boldsymbol{p}'$ is the conjugate operator of $\boldsymbol{p}$ acting on the left. Specifically, they are

$$\begin{aligned} A_0 &= \tfrac{1}{4}t_0(2 + x_0), \quad A_1 = \tfrac{1}{4}t_0(1 + 2x_0), \\ B_0 &= \tfrac{1}{24}t_3(2 + x_3), \quad B_1 = \tfrac{1}{24}t_3(1 + 2x_3), \\ C &= \tfrac{1}{16}[t_1(2 + x_1) + t_2(2 + x_2)], \\ D &= \tfrac{1}{16}[t_2(2x_2 + 1) - t_1(2x_1 + 1)]. \end{aligned} \tag{4}$$

Values of these Skyrme parameters can be found in Ref. [8].

The single-particle potential of a nucleon, which can be calculated from $\partial\epsilon_{\rm pot}/\partial\rho_q$ or $\frac{\partial\epsilon_{\rm pot}/\partial f_q}{\partial\rho_q/\partial f_q}$, is then given by

$$\begin{aligned} U_q(\boldsymbol{r}, \boldsymbol{p}) = {} & 2A_0\rho - 2A_1\rho_q + B_0(\alpha + 2)\rho^{\alpha+1} \\ & - B_1\alpha\rho^{\alpha-1}\left(\rho_n^2 + \rho_p^2\right) - 2B_1\rho^\alpha\rho_q \\ & + 2C\int d^3\boldsymbol{p}'(\boldsymbol{p} - \boldsymbol{p}')^2 f(\boldsymbol{r}, \boldsymbol{p}') \\ & + 2D\int d^3\boldsymbol{p}'(\boldsymbol{p} - \boldsymbol{p}')^2 f_q(\boldsymbol{r}, \boldsymbol{p}') \\ = {} & a_q\boldsymbol{p}^2 - \boldsymbol{b}_q \cdot \boldsymbol{p} + c_q, \end{aligned} \tag{5}$$

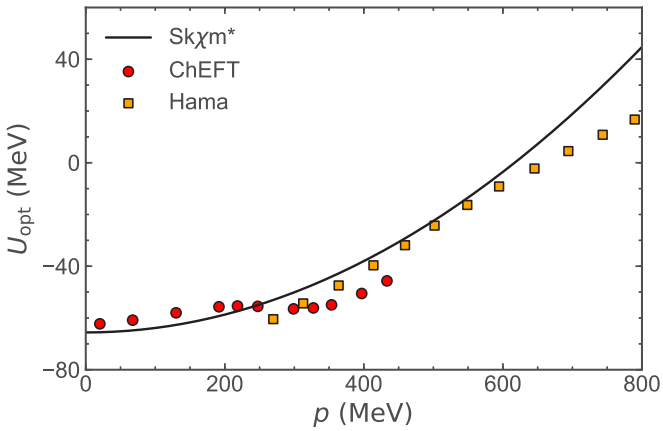


FIG. 1. Momentum dependence of the nucleon single-particle potential in symmetric nuclear matter at saturation density from the Skχm* interaction. Also shown are the optical potential predicted by the chiral effective theory [35] and the empirical optical potential from Hama *et al.* [36,37].

where $q = p, n$, and the coefficients $a_q$, $\boldsymbol{p}_q$, and $c_q$ are given by

$$\begin{aligned} a_q &= 2C\rho + 2D\rho_q, \\ \boldsymbol{b}_q &= 4C\int d^3\boldsymbol{p}'\boldsymbol{p}' f(\boldsymbol{r},\boldsymbol{p}') + 4D\int d^3\boldsymbol{p}'_q\boldsymbol{p}'_q f_q(\boldsymbol{r},\boldsymbol{p}'_q), \\ c_q &= 2A_0\rho - 2A_1\rho_q + B_0(\alpha+2)\rho^{\alpha+1} \\ &\quad - B_1\alpha\rho^{\alpha-1}\left(\rho_n^2+\rho_p^2\right) - 2B_1\rho^\alpha\rho_q \\ &\quad + 2C\int d^3\boldsymbol{p}'\boldsymbol{p}'^2 f(\boldsymbol{r},\boldsymbol{p}') + 2D\int d^3\boldsymbol{p}'_q\boldsymbol{p}'^2_q f_q(\boldsymbol{r},\boldsymbol{p}'_q). \end{aligned} \tag{6}$$

For the potentials of Δ resonances, they are determined from those of nucleons according to the extensively used relations in literatures based on isospin considerations [16],

$$\begin{aligned} U_{\Delta^{++}} &= U_p, \quad U_{\Delta^+} = \tfrac{2}{3}U_p + \tfrac{1}{3}U_n, \\ U_{\Delta^0} &= \tfrac{1}{3}U_p + \tfrac{2}{3}U_n, \quad U_{\Delta^-} = U_n. \end{aligned} \tag{7}$$

For example, we have the coefficients $a_{\Delta^+} = 2a_p/3 + a_n/3$, $\boldsymbol{b}_{\Delta^+} = 2\boldsymbol{b}_p/3 + \boldsymbol{b}_n/3$, and $c_{\Delta^+} = 2c_p/3 + c_n/3$ for the $\Delta^+$ resonance.

Figure 1 shows the momentum dependence of the nucleon single-particle potential in symmetric nuclear matter at saturation density from the Skχm* interaction. For comparison, we also show by filled circles the predictions from the chiral effective field theory [35] and by filled squares the empirical optical potential from Hama *et al.* [36,37]. It is seen that the Skχm* interaction can reasonably describe these nucleon single-particle potentials up to momentum $p \sim 700$ MeV.

From Eq. (5), we find that baryons in the Skχm* interaction can be treated like free particles with the effective mass $m_q^*$, kinetic momentum $\boldsymbol{p}^*$, and energy $E^*$ defined by

$$\begin{aligned} \frac{1}{2m_q^*} &= \frac{1}{2m_q} + a_q, \quad \boldsymbol{p}_q* = \boldsymbol{p}_q - \boldsymbol{\Sigma}_q, \\ E_q^* &= E_q - \Sigma_q^0, \end{aligned} \tag{8}$$

where $\Sigma_q^0 = c_q - \frac{m_q^* b_q^2}{2} + m_q - m_q^*$ and $\boldsymbol{\Sigma}_q = m_q^*\boldsymbol{b}_q$. In terms of these quantities, the kinetic and canonical energies of a baryon can be expressed as $E_q^* = m_q^* + \boldsymbol{p}_q^{*2}/(2m_q^*)$ and $E_q = m_q^* + \boldsymbol{p}_q^{*2}/(2m_q^*) + \Sigma_q^0$, respectively. It should be noted that the total kinetic momentum $\boldsymbol{p}^*$ and energy $E^*$ in an inelastic collision, such as $N + N \leftrightarrow N + \Delta$, are not necessarily conserved due to the difference between initial and final potentials, although the total canonical momentum $\boldsymbol{p}$ and energy $E$ are conserved.

### B. Scattering cross sections and Δ decay width

Following the relativistic Valsov-Uehling-Uhlenbeck (RVUU) model [38,39] used in Ref. [27], we use the baryon-baryon elastic cross sections parameterized in Ref. [40] and the Δ production cross section from the one-boson exchange model [41]. As discussed in Ref. [27], the baryon mean-field potentials modify the Δ production threshold and also the total energy of two colliding nucleons, leading to a change in the Δ production cross section called the threshold effect [26,27]. For the $N + N \to N + \Delta$ reaction in the presence of mean-field potentials, the energy in the final state is

$$\begin{aligned} E_{\rm f} &= m_3^* + m_4^* + \frac{\boldsymbol{p}_3^{*2}}{2m_3^*} + \frac{\boldsymbol{p}_4^{*2}}{2m_4^*} + \Sigma_3^0 + \Sigma_4^0 \\ &= m_3^* + m_4^* + \frac{(\boldsymbol{p}_3^* + \boldsymbol{p}_4^*)^2}{2(m_3^* + m_4^*)} + \frac{\boldsymbol{k}^{*2}}{2\mu_{34}} + \Sigma_3^0 + \Sigma_4^0, \end{aligned} \tag{9}$$

with $m_3^*$ and $\mathbf{p}_3^*$ being the effective mass and kinetic momentum of nucleon, and $m_4^*$ and $\mathbf{p}_4^*$ being those of Δ. The second line with the reduced effective mass $\mu_{34} = m_3^* m_4^*/(m_3^* + m_4^*)$ follows after introducing the relative kinetic momentum $\boldsymbol{k}^* = \boldsymbol{p}_3^* - m_3^*\frac{\boldsymbol{p}_3^* + \boldsymbol{p}_4^*}{(m_3^* + m_4^*)} = -[\boldsymbol{p}_4^* - m_4^*\frac{\boldsymbol{p}_3^* + \boldsymbol{p}_4^*}{(m_3^* + m_4^*)}]$. The threshold energy can then be determined by taking $\boldsymbol{p}_3^* + \boldsymbol{p}_4^* = 0$ and $\boldsymbol{k}^* = 0$ [27], leading to the following invariant threshold energy:

$$\sqrt{s}_{\rm th} = \sqrt{\left(m_3^* + m_4^* + \Sigma_3^0 + \Sigma_4^0\right)^2 - (\boldsymbol{\Sigma}_3 + \boldsymbol{\Sigma}_4)^2}. \tag{10}$$

As an example, for a head-on collision in the local rest frame, i.e., $\boldsymbol{p}_3 + \boldsymbol{p}_4 \simeq 0$, one has $\boldsymbol{b}_{3,4} \simeq 0$. As a result, $\boldsymbol{\Sigma}_{3,4} = 0$ and $\Sigma_{3,4}^0 = c_{3,4} + m_{3,4} - m_{3,4}^*$, and the difference of the total energy and the threshold energy in the frame $\boldsymbol{p}_3^* + \boldsymbol{p}_4^* = 0$ is

$$\begin{aligned} \sqrt{s}_{\rm in} - \sqrt{s}_{\rm th} &\simeq m_1 + m_2 - m_3 - m_4 + \frac{\boldsymbol{p}_1^2}{2m_1^*} \\ &\quad + \frac{\boldsymbol{p}_2^2}{2m_2^*} + c_1 + c_2 - c_3 - c_4, \end{aligned} \tag{11}$$

where $m_1$ and $m_2$ denote the masses of initial two nucleons in the reaction. For nuclear matter at zero temperature and of density $\rho_N = 1.5\rho_0$ and isospin asymmetry $\delta = 0.2$, the Skχm* interaction gives $m_n^* = 687.7$ MeV, $m_p^* = 659.4$ MeV, $c_n = -64.10$ MeV, and $c_p = -77.05$ MeV. Because of the $c_1 + c_2 - c_3 - c_4$ term in Eq. (11), the energy difference is increased (reduced) by 12.95 MeV for the reaction $n + n \to p + \Delta^-(p + p \to n + \Delta^{++})$ reactions. This would lead to

enhanced and suppressed production cross sections for $\Delta^-$ and $\Delta^{++}$ in neutron-rich nuclear matter, respectively, if the scattering amplitudes for these reactions are assumed to be not affected by the medium. Since nucleon effective masses in nuclear medium are less than their bare masses, the energy difference turns out to always increase, leading thus to enhanced $\Delta$ production cross sections in nuclear medium. In particular, for $p_1 = p_2 \approx 370$ MeV, which is roughly the minimum momentum that can produce a $\Delta$ resonance in a head-on nucleon-nucleon collision in vacuum, the energy difference increases by about 60 MeV due to the change of nucleon effective masses, which can lead to a significant enhancement of $\Delta$ production in all channels. Because of $m_n^* > m_p^*$, the effective mass effect enhances $\Delta^{++}$ production more than $\Delta^-$ production. For the $\pi^-/\pi^+$ ratio in heavy-ion collisions, there is therefore a competition between the effects of the baryon effective masses and the momentum-independent part of baryon mean-field potentials.

For a $\Delta$ resonance of mass $m_\Delta$ and in isospin state $m_T$, we take its decay width to have the following form [42]:

$$\Gamma = \sum_{m_t} \frac{0.47 C q^3}{m_\pi^2 + 0.6 q^2}, \tag{12}$$

where $m_t$ is the isospin state of the emitted pion; $C = |\langle \frac{3}{2}, m_T | 1, m_t; \frac{1}{2}, m_T - m_t \rangle|^2$ is the square of the Clebsch-Gordan coefficient from the isospin coupling; and $q$ is the magnitude of the momentum of pion or nucleon in the rest frame of $\Delta$ and is given by

$$q = \frac{\sqrt{\left[m_\Delta'^2 - (m_N' + m_\pi)^2\right]\left[m_\Delta'^2 - (m_N' - m_\pi)^2\right]}}{2m_\Delta'}. \tag{13}$$

Here the in-medium mass $m_q'$ is defined as $E_q(p_q = 0)$ to include the effect of mean-field potentials on the $\Delta$ decay width. The spectral function of $\Delta$ resonance is then given by

$$\mathcal{A}(m') = \frac{1}{\mathcal{N}} \frac{4 m_0'^2 \Gamma(m')}{\left(m'^2 - m_0'^2\right)^2 + m_0'^2 \Gamma^2(m')}, \tag{14}$$

where $m_0'$ is the pole mass (1.232 GeV) of the $\Delta$ resonance shifted by the mean-field potential and $\mathcal{N}$ is the normalization factor determined by $\int \frac{dm}{2\pi} \mathcal{A}(m) = 1$.

### C. Detailed balance relations in nuclear medium

In the last section, we have introduced the $\Delta$ production cross section and decay width in nuclear medium. For the inverse processes, they can be determined by the detailed balance relations.

Considering the reaction $N + N \to N + \Delta$ of nucleons and $\Delta$ in certain isospin states and labeling the initial two nucleons by 1 and 2 and the final nucleon and $\Delta$ by 3 and 4, respectively, the total cross section in the nonrelativistic approximation can be expressed as

$$\sigma_{NN\to N\Delta} = \int \frac{dm_4}{2\pi} \mathcal{A}(m_4) \int \frac{d^3\boldsymbol{p}_3^*}{(2\pi)^3} \frac{d^3\boldsymbol{p}_4^*}{(2\pi)^3} \frac{\overline{|\mathcal{M}_{NN\to N\Delta}|^2}}{|\boldsymbol{v}_1 - \boldsymbol{v}_2|} \times (2\pi)^4 \delta^4(p_1 + p_2 - p_3 - p_4), \tag{15}$$

where $\overline{|\mathcal{M}|^2}$ is the squared invariant scattering amplitude after averaging over the spins of initial particles and summing over the spins of final particles, $m_4$ is the mass of $\Delta$, $p_i(p_i^*)$ is the canonical (kinetic) four-momentum of particle $i$ ($i = 1, 2, 3, 4$), and $|\boldsymbol{v}_1 - \boldsymbol{v}_2| = |\boldsymbol{p}_1^*/m_1^* - \boldsymbol{p}_2^*/m_2^*|$ is the relative velocity of particles 1 and 2. In terms of their relative kinetic momentum,

$$\boldsymbol{k}_i^* = \frac{\boldsymbol{p}_1^*}{m_1^*} - m_1^* \frac{\boldsymbol{p}_1^* + \boldsymbol{p}_2^*}{m_1^* + m_2^*} = -\left(\frac{\boldsymbol{p}_2^*}{m_2^*} - m_2^* \frac{\boldsymbol{p}_1^* + \boldsymbol{p}_2^*}{m_1^* + m_2^*}\right), \tag{16}$$

and evaluating the integral in the center-of-mass frame, the cross section becomes

$$\begin{aligned}\sigma_{NN\to N\Delta} &= \frac{1}{(2\pi)^3} \int dm_4 \mathcal{A}(m_4) \int 4\pi k_f^{*2} dk_f^* \\ &\quad \times \frac{\overline{|\mathcal{M}_{NN\to N\Delta}|^2}}{k_i^*/\mu_i} \delta\left(E_f' - \frac{k_f^{*2}}{2\mu_f}\right) \\ &= \frac{1}{2\pi^2} \frac{\mu_i}{k_i^*} \int dm_4 \mathcal{A}(m_4) k_f^* \mu_f \overline{|\mathcal{M}_{NN\to N\Delta}|^2},\end{aligned} \tag{17}$$

where $\mu_i = m_1^* m_2^*/(m_1^* + m_2^*)$ is the reduced effective mass of initial particles and $\mu_f = m_3^* m_4^*/(m_3^* + m_4^*)$ and $k_f^*$ are, respectively, the reduced effective mass of final particles and their relative momentum introduced below Eq. (9), which can be determined from energy and momentum conservations. The mass of $\Delta$ resonance produced in the reaction $N + N \to N + \Delta$ can have various values with their distribution given by its spectral function $\mathcal{A}(m_\Delta)$ [Eq. (14)] and is determined according to the probability

$$P(m_\Delta) = \frac{\mathcal{A}(m_\Delta) k_f^* \mu_f}{\int dm_\Delta \mathcal{A}(m_\Delta) k_f^* \mu_f}. \tag{18}$$

For a $\Delta$ resonance of mass $m_\Delta$, its absorption cross section by a nucleon in nucleon medium via the inverse reaction $N + \Delta \to N + N$ is given by

$$\sigma_{N\Delta\to NN} = \frac{1}{\pi} \frac{k_i^*}{k_f^*} \mu_i \mu_f \overline{|\mathcal{M}_{N\Delta\to NN}|^2}. \tag{19}$$

By comparing Eq. (17) and (19) and using the relation $\overline{|\mathcal{M}_{NN\to N\Delta}|^2} = 2\overline{|\mathcal{M}_{N\Delta\to NN}|^2}$, we obtain the detailed balance relation as

$$\sigma_{N\Delta\to NN} = \frac{\sigma_{12}}{2(1+\delta_{12})} \frac{k_i^{*2}}{k_f^*} \frac{\mu_f}{\int \frac{dm'}{2\pi} k_f^{*\prime} \mu_f' \mathcal{A}(m')}. \tag{20}$$

For the total decay width of a $\Delta$ in nuclear medium, it is already given in Eq. (12) as the sum of its partial widths. As to the cross section of the inverse process $\pi + N \to \Delta$ in a particular isospin channel, we can obtain it from the partial decay width of the $\Delta$ in this isospin channel by using the detailed balance relation as described in the following. Since the $N + \pi$ center-of-mass frame cannot be trivially defined when nucleons and pions are treated differently with nucleons as nonrelativistic particles and pions as relativistic particles, we therefore treat both $\Delta$ decay and pion absorption in the nuclear matter frame and express the decay width of $\Delta$ in terms of the squared invariant scattering amplitude

$\overline{|\mathcal{M}_{\Delta\to N\pi}|^2}$ averaged over the spin of $\Delta$ and summed over the spin of nucleon, that is,

$$\Gamma = \int \frac{d^3\boldsymbol{p}_N^*}{(2\pi)^3}\frac{d^3\boldsymbol{p}_\pi}{(2\pi)^3}\frac{\overline{|\mathcal{M}_{\Delta\to N\pi}|^2}}{2\omega}(2\pi)^4\delta^4(p_N + p_\pi - p_\Delta), \tag{21}$$

with $\omega(p) = \sqrt{m_\pi^2 + p^2}$ being the pion energy. Taking the direction of $\boldsymbol{P}^* = \boldsymbol{p}_N^* + \boldsymbol{p}_\pi = \boldsymbol{p}_\Delta - \boldsymbol{\Sigma}_N$ as the $z$ axis, the decay width can be rewritten as

$$\begin{aligned}\Gamma &= \frac{1}{8\pi^2}\int d^3\boldsymbol{p}_\pi \frac{\overline{|\mathcal{M}_{\Delta\to N\pi}|^2}}{\omega} \\ &\quad\times\delta\left(E_\Delta - m_N^* - \frac{(\boldsymbol{P}^* - \boldsymbol{p}_\pi)^2}{2m_N^*} - \Sigma_N^0 - \omega\right) \\ &= \frac{1}{4\pi}\int p_\pi^2 dp_\pi \frac{\overline{|\mathcal{M}_{\Delta\to N\pi}|^2}}{\omega}\frac{m_N^*}{P^* p_\pi} \\ &= \frac{m_N^*\overline{|\mathcal{M}_{\Delta\to N\pi}|^2}}{4\pi P^*}\int \frac{p_\pi}{\omega}dp_\pi \\ &= \frac{m_N^*\overline{|\mathcal{M}_{\Delta\to N\pi}|^2}}{4\pi P^*}[\omega(p_{\max}) - \omega(p_{\min})],\end{aligned} \tag{22}$$

where $p_{\min}$ and $p_{\max}$ are the allowed minimum and maximum pion momenta and can be analytically determined from the energy conservation in $\Delta$ decay and the condition of $-1 \leqslant \cos\theta \leqslant 1$, with $\theta$ being the angle between the pion momentum and the $z$ axis. In the above, we have assumed that the squared invariant transition matrix element $\overline{|\mathcal{M}_{\Delta\to N\pi}|^2}$ is independent of the pion momentum $\boldsymbol{p}_\pi$. The decay width of $\Delta$ of a certain charge state can be obtained from Eq. (22) by taking into consideration of appropriate isospin factors.

The spin-averaged cross section for the process $N + \pi \to \Delta$ is given by

$$\begin{aligned}\sigma_{N\pi\to\Delta} &= \int \frac{dm}{2\pi}\mathcal{A}(m)\int \frac{d^3\boldsymbol{p}_\Delta^*}{(2\pi)^3}\frac{\overline{|\mathcal{M}_{N\pi\to\Delta}|^2}}{2\omega|v_N - v_\pi|} \\ &\quad\times(2\pi)^4\delta^4(p_N + p_\pi - p_\Delta), \\ &= \frac{\mathcal{A}(m)\overline{|\mathcal{M}_{N\pi\to\Delta}|^2}}{2\omega|v_N - v_\pi|}\frac{1}{\left|1 - \frac{p_\Delta}{m_\Delta}\right|},\end{aligned} \tag{23}$$

where $\boldsymbol{v}_N = \boldsymbol{p}_N^*/m_N^*$ and $\boldsymbol{v}_\pi = \boldsymbol{p}_\pi/\omega$. Using the relation $2\overline{|\mathcal{M}_{\Delta\to N\pi}|^2} = \overline{|\mathcal{M}_{N\pi\to\Delta}|^2}$, we then have

$$\sigma_{N\pi\to\Delta} = \frac{4\pi P^*}{m_N^*|\boldsymbol{v}_N - \boldsymbol{v}_\pi|\left|1 - \frac{p_\Delta}{m_\Delta}\right|}\frac{\mathcal{A}(m_\Delta)\Gamma(m_\Delta)}{\omega(p_\pi)[\omega(p_{\max}) - \omega(p_{\min})]}, \tag{24}$$

where the $\Delta$ mass is determined by $m_\Delta = P^2/2(E - a_\Delta P^2 + \boldsymbol{b}_\Delta\cdot\boldsymbol{P} - c_\Delta)$ with $E$ and $\boldsymbol{P}$ being, respectively, the total energy and momentum of the colliding nucleon and pion. We note again that both $\sigma_{N\pi\to\Delta}$ and $\Gamma(m_\Delta)$ refer to the same isospin channel of the processes $\Delta \leftrightarrow N\pi$, while the $\Delta$ width in $\mathcal{A}(m_\Delta)$ given in Eq. (14) refers to its total width.

## III. RESULTS AND DISCUSSION

In this section, we present results obtained from calculations using the $\chi$BUU transport model for pion production in a hot neutron-rich nuclear matter in a box and from heavy-ion collisions. They are obtained by solving the BUU equation using the test particle method [40,43]. In this method, the time evolution of baryon phase-space distribution functions is described by the following equations of motion for test baryons:

$$\begin{aligned}\dot{\boldsymbol{r}} &= \frac{\boldsymbol{p}^*}{m^*}, \\ \dot{\boldsymbol{p}} &= \nabla\left(m^* + \frac{\boldsymbol{p}^{*2}}{2m^*} + \Sigma^0\right),\end{aligned} \tag{25}$$

with the baryon mean-field potentials calculated self-consistently according to the local nucleon and $\Delta$ distributions determined from corresponding test particles. The same is for the phase-space distribution functions of pions except that the test pions move freely with the constant velocity $\boldsymbol{p}/\sqrt{m_\pi^2 + p^2}$ as we have neglected the pion potentials in the present study.

For particle collisions, they are treated using the standard geometric method described in Ref. [40]. However, instead of using the parallel ensemble method, in which only physical particles in each event can collide although particles from many parallel events are used as the test particles for calculating the mean-field potentials, we adopt the partition method [44] by using in addition $N_{\rm T}$ test particles for a physical particle in an event and reducing accordingly all scattering cross sections by $N_{\rm T}$. As to the $\Delta$ decay probability in each time step $dt$, it is determined by its width according to

$$P = 1 - \exp(-\Gamma dt). \tag{26}$$

For both box and heavy-ion collisions calculations discussed in the following, we use $N_{\rm T} = 10$ and $dt = 0.1\,{\rm fm}/c$.

### A. Pion production in a box

As in Ref. [45], we first study the role of baryon mean-field potentials in the energy conservation condition of collision and decay processes and their effect on pion production in a hot neutron-rich matter. Specifically, we study the final equilibrium numbers of $N$, $\Delta$, and $\pi$ for the two cases of with and without baryon mean-field potentials in the energy conservation condition.

For a static and uniform hadronic matter in a box, the baryon vector potentials $\boldsymbol{b}_i$ due to the flow effect are absent. For simplicity, we ignore the quantum nature of $N$, $\Delta$, and $\pi$, and take their momentum distributions at thermal equilibrium to be Boltzmann-like. For pions and nucleons, their momentum distributions at temperature $T$ are then given by

$$f_i(\boldsymbol{p}_i) = \frac{g_i}{(2\pi)^3}\exp\left[-\frac{E_i - \mu_i}{T}\right], \tag{27}$$

where $i = n, p, \pi^+, \pi^0, \pi^-$, $g_i = 1(2)$ is the spin degeneracy of pion (nucleon), $\mu_i$ is the chemical potential of particle $i$, and $E_i$ is its energy. For $\Delta$ resonances with mass distributions,

TABLE I. Temperature $T$, chemical potentials of neutron $\mu_n$ and proton $\mu_p$, multiplicities of nucleons, $\Delta$s, and pions, pionlike particle multiplicity $\pi_{\rm like}$, and effective charged pion ratio $(\pi^-/\pi^+)_{\rm like}$ in initial and final states in the "free" case (see text for details) from thermal model calculations.

| | $T$ (MeV) | $\mu_n$(MeV) | $\mu_p$(MeV) | $N$ | $Z$ | $\Delta^{++}$ | $\Delta^+$ | $\Delta^0$ | $\Delta^-$ | $\pi^+$ | $\pi^0$ | $\pi^-$ | $\pi_{\rm like}$ | $(\pi^-/\pi^+)_{\rm like}$ |
|---|---|---|---|---|---|---|---|---|---|---|---|---|---|---|
| Initial | 60 | 891.7 | 865.6 | 134.1 | 96.9 | 1.12 | 1.67 | 2.49 | 3.72 | 0.79 | 1.22 | 1.88 | 12.9 | 2.61 |
| Final (free) | 47.2 | 934.6 | 916.7 | 140.6 | 96.2 | 0.42 | 0.61 | 0.89 | 1.30 | 0.28 | 0.40 | 0.59 | 4.48 | 2.44 |

their momentum distributions are

$$f_i(\boldsymbol{p}_i) = 4\int \frac{dm}{(2\pi)^4}\mathcal{A}(m)\exp\left[-\frac{E_i-\mu_i}{T}\right], \tag{28}$$

where $i = \Delta^{++}, \Delta^+, \Delta^0, \Delta^-$, and the factor 4 is due to the spin degeneracy of $\Delta$.

For $N$, $\Delta$, and $\pi$ in chemical equilibrium, their chemical potentials satisfy following relations:

$$\begin{aligned} \mu_{\Delta^{++}} &= 2\mu_p - \mu_n, \quad \mu_{\Delta^+} = \mu_p, \\ \mu_{\Delta^0} &= \mu_n, \quad \mu_{\Delta^-} = 2\mu_n - \mu_p, \\ \mu_{\pi^+} &= \mu_p - \mu_n, \quad \mu_{\pi^0} = 0, \\ \mu_{\pi^-} &= \mu_n - \mu_p. \end{aligned} \tag{29}$$

Given the temperature $T$, baryon density $\rho_B$, and isovector density $\rho_I = \rho_p - \rho_n + \rho_{\Delta^{++}} + \rho_{\Delta^+}/3 - \rho_{\Delta^0}/3 - \rho_{\Delta^-}$, the mean-field potentials of baryons and their numbers can be obtained by solving above questions iteratively.

In our box calculation, all particles are confined in a cubic box of volume $10\times10\times10$ fm$^3$ with periodic boundary conditions, and both the Coulomb interaction and the Pauli blocking effect are neglected. Initially, the temperature, baryon, and isovector densities are taken to be $T = 60$ MeV, $\rho = 0.24$ fm$^{-3}$, and $\rho_I = 0.096$ fm$^{-3}$, respectively, which resemble the conditions of the dense matter in intermediate-energy heavy-ion collisions where most pions are produced [22]. The resulting parameters in Eq. (6) for nucleon mean-field potentials are $a_p = 0.2617$ GeV$^{-1}$, $c_p = -59.87$ MeV, $a_n = 0.2360$ GeV$^{-1}$, and $c_n = -50.34$ MeV. The initial numbers of $N$, $\Delta$, and $\pi$ of various charges are shown in the first row of Table I. For the initial momentum spectra, which are determined by Eqs. (27) and (28), they are shown by solid lines in Figs. 2(a), 2(b) and 2(c) for neutron, $\Delta^-$, and $\pi^-$, respectively.

Evaluating baryon mean fields using test particles from 20 parallel events and averaging results from 20 such parallel ensemble calculations, we have studied the time evolutions of $\Delta$ and $\pi$ numbers for the two cases of with and without baryon mean-field potentials in the energy conservation condition of scattering and decay processes. As shown in Figs. 3 and 4, the numbers of $\Delta$ and $\pi$ in the Sk$\chi$m$^*$ case remain almost unchanged except for small statistical fluctuations due to the finite numbers of test particles and events used in the calculations. In the free case, without including the baryon mean-field potentials in the energy conservation conditions of scattering and decay processes, the numbers of $\Delta$ and $\pi$ decrease with time. The final equilibrium numbers in the system for the free case can also be determined by thermal model calculations using the conditions of energy, baryon density, and isospin density conservations. These results are given in the second rows of Table I and are also shown in Figs. 3 and 4 by open circles. It is seen that the box calculations well reproduce the thermal model results with a deviation less than ~2%. The momentum distributions of neutron, $\Delta^-$, and $\pi^-$ in the box at $t = 50$ fm/$c$ for the two cases are shown by solid and open circles in Figs. 2(a), 2(b) and 2(c), respectively, while corresponding momentum spectra from the thermal model are exhibited as curves. It is seen that in both cases the $N$-$\Delta$-$\pi$ system is at the expected thermal equilibrium states.

We note that including mean-field potentials in the energy conservation condition in elementary reactions is also needed to guarantee the conservation of the total energy of the system,

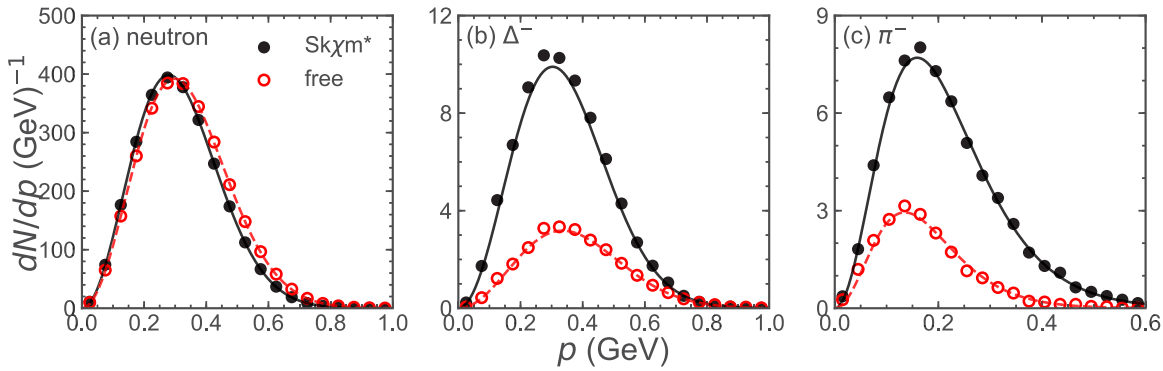


FIG. 2. Momentum distributions of neutron (left panel), $\Delta^-$ (middle panel), and $\pi^-$ (right panel) in a box at $t = 50$ fm/$c$. Solid lines are theoretical momentum distributions from the thermal model with the inclusion of baryon potentials at $T = 60$ MeV, and dashed lines are those in the final state of the "free" case (see text for details). Solid circles are results from the $\chi$BUU model including the effect of baryon potentials in the energy conservation condition in elementary reactions (Sk$\chi$m$^*$), and open circles are those without including this effect (free).

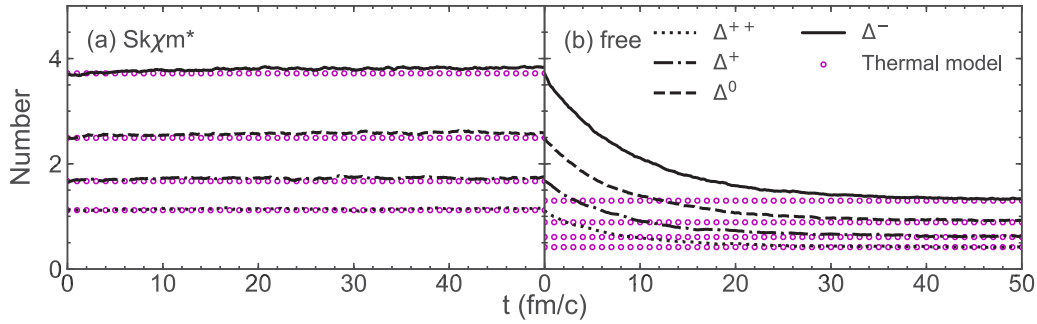


FIG. 3. Time evolutions of Δ numbers in box calculations for the two cases of with and without mean-field potentials in the energy conservation condition of scattering and decay processes. For comparison, results from the thermal model are shown as open cycles.

which can be evaluated according to

$$E = \sum_i \left( m_i + \frac{p_i^2}{2m_i} + \frac{1}{2}U_i \right) + \sum_j \sqrt{m_\pi^2 + p_j^2} + E_{\rm r}, \quad (30)$$

with $i = n, p, \Delta^{++}, \Delta^{+}, \Delta^{0}, \Delta^{-}$, and $j = \pi^+, \pi^0, \pi^-$. Here the rearrangement energy $E_{\rm r}$ is given by

$$E_{\rm r} = -\frac{\alpha}{2} \int d^3\mathbf{r} \rho^\alpha \left[ B_0 \rho^2 - B_1 \left( \rho_p^2 + \rho_n^2 \right) \right] \quad (31)$$

with the integration over the volume of the box. It is found that with an initial total energy of 237.2 GeV, the total energy increases by only 120 MeV after 50 fm/$c$ for the Sk$\chi$m$^*$ case but by 1.02 GeV for the free case.

It is known in heavy-ion collisions that the effective pion number, which includes all pionlike particles, changes very little after the colliding nuclear matter reaches maximum compression [46,47]. In our case, the effective pion number is given by the sum of Δ resonance and pion numbers, i.e., $\pi_{\rm like} = \pi^- + \pi^0 + \pi^+ + \Delta^{++} + \Delta^+ + \Delta^0 + \Delta^-$, as shown in Table I. Also shown in Table I is the effective charged pion ratio $(\pi^-/\pi^+)_{\rm like}$ defined as

$$(\pi^-/\pi^+)_{\rm like} = \frac{\pi^- + \Delta^- + \Delta^0/3}{\pi^+ + \Delta^{++} + \Delta^+/3}. \quad (32)$$

Comparing results with and without baryon potentials, we find that omitting the baryon potentials in the energy conservation condition significantly decreases the effective pion number by a factor of 3 but decreases the effective charged pion ratio by only about 6.5%. The reduction of total pion number by baryon mean-field potentials can be understood from the nucleon momentum distribution

$$f(p) \propto \exp\left( -\frac{p^2}{2m^*T} \right) \exp\left( \frac{\mu - m - c}{T} \right). \quad (33)$$

It shows that removing baryon potentials increases the effective mass of baryons and thus decreases the temperature of the system compared to the Sk$\chi$m$^*$ case as shown in Table I, leading to a significant reduction of effective pion numbers. The small decrease of the effective pion ratio can be understood from the following relation based on thermal and chemical equilibrium,

$$\frac{\pi^-}{\pi^+} = \exp\left[ \frac{2(\mu_n - \mu_p)}{T} \right] = \frac{N^2}{Z^2} \left( \frac{m_p^*}{m_n^*} \right)^3 \exp\left[ \frac{2(c_n - c_p)}{T} \right], \quad (34)$$

where $N$ and $Z$ are the neutron and proton numbers, respectively. For the Sk$\chi$m$^*$ energy density functional, $m_n^*$ ($c_n$) is larger than $m_p^*$ ($c_p$) in neutron-rich nuclear matter. Compared with the case without baryon potentials, $(m_p^*/m_n^*)^3$ increases but $\exp[\frac{2(c_n-c_p)}{T}]$ decreases after including the potentials. The cancellation of the two contributions then leads to a smaller decrease of effective pion ratio.

We note that the decrease of the effective pion ratio after removing baryon potentials is much smaller than that based on the RVUU model, where the effective pion ratio is reduced by 26.7% [45]. As discussed in Sec. II B, the baryon mean-

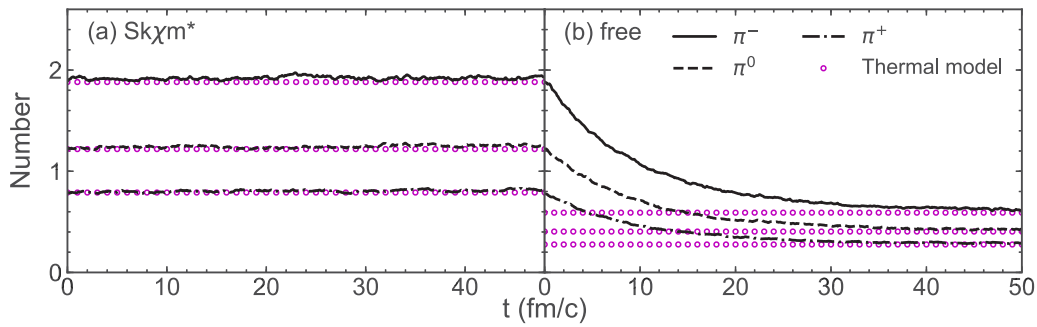


FIG. 4. Same as Fig. 3 for $\pi$ numbers.

field potentials can lead to a change in the energy difference between the center-of-mass energy of two colliding nucleons and the threshold energy for $\Delta$ production and thus affect the $\Delta$ production cross sections in nuclear medium. For a system confined in a box as in the present study, changing these cross sections only influences the time for the system to reach a new equilibrium after neglecting the potentials but does not affect the final equilibrium particle numbers. However, in nuclear collisions, where thermal and chemical equilibriums may not be completely reached, the change of cross sections could have a large effect on the final pion number and the charged pion ratio [27]. In next section, we further study such nonequilibrium effects in heavy-ion collisions.

### B. Heavy-ion collisions

In this section, we employ the transport model to study pion production in heavy-ion collisions. For the initial positions of nucleons inside in each nucleus, they are distributed according to the density distribution obtained from the self-consistent Hartree-Fock calculation using the Sk$\chi$m$^*$ interaction. As to their momentum-space distributions, we use the Fermi gas model with the Fermi momentum determined by the local density. Unlike the box calculation, the effect of electromagnetic fields and Pauli blocking are both included. The electric and magnetic fields acting on a charged particle $i$ are evaluated according to

$$\boldsymbol{E}(\boldsymbol{r}_i) = \frac{e}{4\pi N_{\rm test}} \sum_{j\neq i} q_j \frac{\boldsymbol{r}_{ij}}{r_{ij}^3},$$
$$\boldsymbol{B}(\boldsymbol{r}_i) = \frac{e}{4\pi N_{\rm test}} \sum_{j\neq i} q_j \frac{\boldsymbol{v}_j \times \boldsymbol{r}_{ij}}{r_{ij}^3}, \quad (35)$$

where $e^2/(4\pi) = 1/137$, $\boldsymbol{r}_{ij} = \boldsymbol{r}_i - \boldsymbol{r}_j$, $\boldsymbol{v}_j$ is the velocity of particle $j$, $q_j$ is its electric charge in units of $e$, and $N_{\rm test}$ is the number of test particles used for representing a physical particle in the calculation. Here the index $j$ runs over all test particles. In all collision (or decay) processes, the Pauli blocking for final-state baryons is included via the same method used in the RVUU model [27,40,48,49], except that the phase-space radii $\Delta r$ and $\Delta p$ are taken to be 1.5 fm and 150 MeV, respectively.

In the following, we show results obtained with mean-field potentials calculated using test particles from 20 parallel events as in the box calculations and from averaging 20 and 300 such parallel ensemble calculations for $^{197}$Au + $^{197}$Au collisions at $E/A = 400$ MeV and Sn+Sn collisions at $E/A = 270$ MeV, respectively.

#### 1. $^{197}$Au + $^{197}$Au *collisions at* $E/A = 400$ *MeV*

We first study central $^{197}$Au + $^{197}$Au collisions at incident energy of $E/A = 400$ MeV and compare the results with experimental data measured by the FOPI Collaboration [50]. Figure 5 shows the time evolutions of the effective $\pi^-$ and $\pi^+$ numbers, namely $(\pi^-)_{\rm like} = \pi^- + \Delta^- + \Delta^0/3$ and $(\pi^+)_{\rm like} = \pi^+ + \Delta^{++} + \Delta^+/3$, in collisions at the impact parameter of 1 fm for the free case without including the effect of baryon mean-field potentials in treating their collisions and

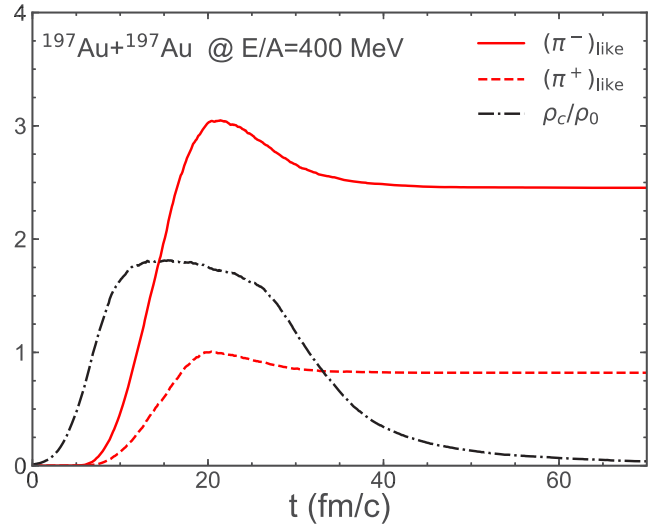


FIG. 5. Time evolutions of the central density $\rho_c$ and effective $\pi^-$ and $\pi^+$ numbers in Au + Au collisions at impact parameters of 1 fm and incident energy of $E/A = 400$ MeV. The mean-field potential effects in the collision terms are not included.

decays, although it is included in their propagations. The central nucleon density $\rho_c$ divided by the saturation density in the dinuclear system is also shown as the black dash-dotted line. It is seen that pionlike particles are mostly produced during the high-density stage and their numbers change very little during later expansion of the system. The final charged pion numbers and ratio $\pi^-/\pi^+$ are listed in the second column (free/$A = 0$) of Table II together with their experimental values measured by the FOPI Collaboration shown in the first column [50]. The theoretical results in this case are seen to well reproduce the charged pion ratio but underestimate the total charged pion yield by about 13%.

We further include mean-field potentials of baryons in determining the collision kinematics and list the results in the third column (Sk$\chi$m$^*/A = 0$) in Table II. Similar to the case of box calculations, the inclusion of mean-field potential effects on the collision kinematics increases both $\pi^-$ and $\pi^+$ numbers by a factor of about 3, although the charged pion ratio remains almost unchanged. To reproduce the experimental data, we follow Ref. [27] by taking into account the medium modification of $\Delta$ production cross section and introduce the

TABLE II. $\pi^-$ and $\pi^+$ yields in $^{197}$Au + $^{197}$Au collisions at the impact parameter of 1 fm and the incident energy of $E/A = 400$ MeV. Experimental data from the FOPI Collaboration [50] are also listed for comparison.

| | FOPI [50] | Free | Sk$\chi$m$^*$ | |
|---|---|---|---|---|
| | | $A = 0$ | $A = 0$ | $A = 1.9$ |
| $\pi^-$ | 2.80(14) | 2.70(3) | 7.84(4) | 2.96(2) |
| $\pi^+$ | 0.95(8) | 0.90(2) | 2.57(2) | 0.92(1) |
| $\pi^- + \pi^+$ | 3.75(22) | 3.60(5) | 10.41(6) | 3.88(3) |
| $\pi^-/\pi^+$ | 2.95(29) | 3.02(6) | 3.05(3) | 3.2(5) |

following density dependence:

$$\sigma_{NN\to N\Delta}(\rho) = \sigma_{NN\to N\Delta}(0)\exp(-A\rho_N/\rho_0), \quad (36)$$

where the $\rho_N$ is the nucleon density and $A$ is a fitting parameter. Cross sections for the inverse reactions are accordingly modified through the detailed balance relation introduced in Sec. II C. We find that taking $A = 1.9$ in the Sk$\chi$m$^*$ case, our model can well reproduce the experimentally measured total charged pion yield. With the density-dependent cross sections, the resulting charged pion ratio is sightly increased by about 5% and becomes 3.2, which is consistent with the experimental value within the error bar [50]. These results thus provide an empirical validation of the behavior of nuclear symmetry energy at high density predicted by the Sk$\chi$m$^*$ energy density functional.

The significant increase of the pion yield due to the threshold effect is consistent with previous results from the RVUU model based on the relativistic NL$\rho$ mean-field model [27]. In both studies, this is because the smaller baryon effective masses in nuclear medium increase the difference between the collision energy of two nucleons and the threshold energy for $\Delta$ production. The small change in the charged pion ratio is, however, in stark contrast with the RVUU model calculations, which shows a much larger change, and this is due to the fact that in neutron-rich nuclear matter, one has $m_n^* > m_p^*$ in the Sk$\chi$m$^*$ energy density functional but $m_n^* = m_p^*$ in the NL$\rho$ model. As discussed in Sec. II B, a positive neuron-proton effective mass splitting would lead to a smaller charged pion ratio.

### 2. $^{132}$Sn + $^{124}$Sn *and* $^{108}$Sn + $^{112}$Sn *collisions at* $E/A = 270$ *MeV*

Including both the effect of baryon mean-field potentials on scattering and decay processes and the medium modification of $\Delta$ production cross sections, we further study pion production in $^{132}$Sn + $^{124}$Sn and $^{108}$Sn + $^{112}$Sn collisions at the incident energy of $E/A = 270$ MeV and the impact parameter of 3 fm, which is being studied experimentally by the SPiRIT Collaboration at the Radioactive Isotope Beam Facility (RIBF) at RIKEN in Japan. As in Au+Au collisions at $E/A = 400$ MeV studied in the previous subsection, pions are mostly produced during the compression stage of the reactions, which can lead to a maximum central density of 0.27/fm$^3$ (1.7 $\rho_0$), and their effective numbers remain essentially constant during the expansion of the system. The obtained total $\pi^-$ and $\pi^+$ numbers and the charged pion ratio $\pi^-/\pi^+$ are, respectively, 0.273, 0.136, and 2.01 for $^{108}$Sn + $^{112}$Sn collisions and 0.508, 0.109, and 4.68 for $^{132}$Sn + $^{124}$Sn collisions. The charged pion ratio $\pi^-/\pi^+$ in the neutron-richer system ($^{132}$Sn + $^{124}$Sn) is thus larger as a result of more neutron-neutron collisions. As in Ref. [31], we select charged pions with the polar angles $\theta_{\rm cm}$ of their momenta relative to the incident beam direction lying in the range of $60^\circ < \theta_{\rm cm} < 120^\circ$ and shows their kinetic energy spectra in Fig. 6. In both collisions, the charged pion ratio decreases with pion kinetic energy. The very large $\pi^-/\pi^+$ ratio at low kinetic energy is mainly due to the Coulomb potential, which is repulsive for $\pi^+$ but attractive for $\pi^-$ [32].

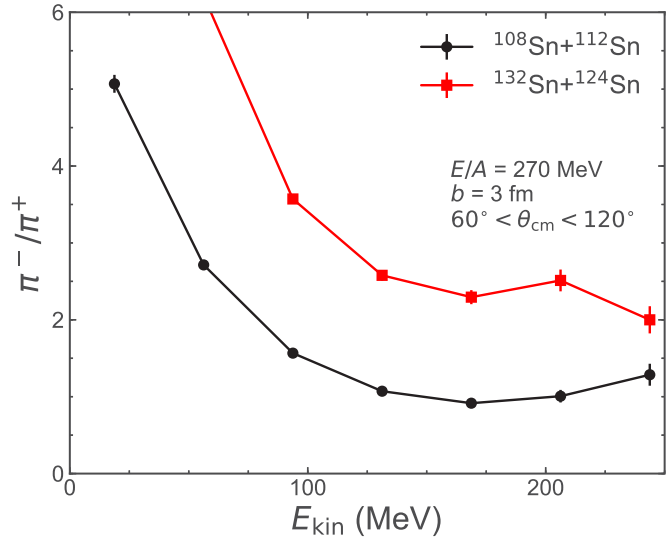


FIG. 6. $\pi^-/\pi^+$ ratios as functions of pion kinetic energy from central ($b = 3$ fm) collisions of $^{132}$Sn + $^{124}$Sn and $^{108}$Sn + $^{112}$Sn at the incident energy of $E/A = 270$ MeV. $\theta_{\rm cm}$ is the polar angle of pion momentum relative to the incident beam direction.

To reduce the Coulomb effect as well as other isospin-independent effects, the double $[(\pi^-/\pi^+)_{132+124}/(\pi^-/\pi^+)_{108+112}]$ [51] and subtracted $[(\pi^-/\pi^+)_{132+124} - (\pi^-/\pi^+)_{108+112}]$ [31] $\pi^-/\pi^+$ ratios of the two reaction systems have been proposed as better probes of nuclear symmetry energy. In Fig. 7, we show the double and subtracted $\pi^-/\pi+$ ratios as functions of the pion kinetic energy. We find that the double ratio is flat with respect to the pion kinetic energy, while the subtracted ratio decreases with increasing pion kinetic energy. Because of its negative charge, $\pi^-$ should be easier to detect than $\pi^+$. Therefore, the isoscaling ratio $\pi_{132+124}/\pi_{108+112}$ of $\pi^-$ from these two reactions may be a

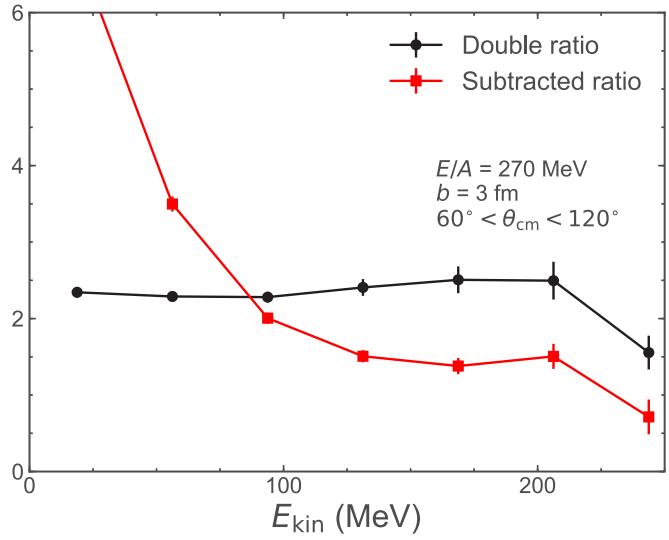


FIG. 7. Same as Fig. 6 for double $[(\pi^-/\pi^+)_{132+124}/(\pi^-/\pi^+)_{108+112}]$ and subtracted $[(\pi^-/\pi^+)_{132+124} - (\pi^-/\pi^+)_{108+112}]$ $\pi^-/\pi^+$ ratios.

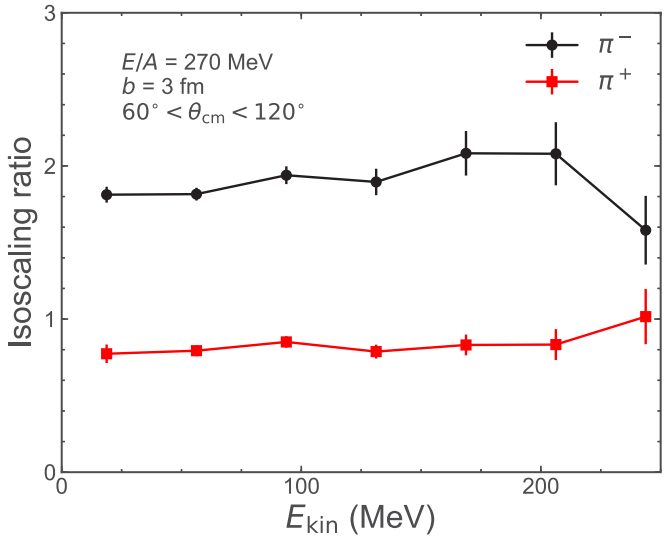


FIG. 8. Same as Fig. 6 for isoscaling $[\pi_{132+124}/\pi_{108+112}]$ ratios of $\pi^-$ and $\pi^+$.

more sensitive observable for probing the nuclear symmetry energy at high density [31]. Figure 8 shows the isoscaling ratio of $\pi^-$ and $\pi^+$ for these two reactions, and it indicates that both are flat with respect to the pion kinetic energy with the isoscaling ratio of $\pi^-$ larger than that of $\pi^+$.

We note that if the effect of mean-field potentials is not included in collisions and decays, the total $\pi^-$ and $\pi^+$ numbers and the charged pion ratio $\pi^-/\pi^+$ would, respectively, be 0.126, 0.063, and 2.01 for $^{108}$Sn + $^{112}$Sn collisions and 0.233, 0.053, and 4.40 for $^{132}$Sn + $^{124}$Sn collisions. As in Au+Au collisions at $E/A = 400$ MeV, the charged pion ratio is only slightly affected by the effect of baryon mean-field potentials in treating their collisions and decays. Although this is also the case for the kinetic energy spectra of double, subtracted, and isoscaling ratios, the total pion number is, however, reduced by about a factor of 2 without including the baryon mean-field potentials in their collisions and decays.

## IV. SUMMARY

We have developed a BUU transport model based on the Sk$\chi$m$^*$ interaction, which is constructed from fitting the equation of state and nuclear effective masses predicted by the chiral effective theory as well as the binding energies of finite nuclei. This $\chi$BUU model is then used to study the effect of energy conservation in the collision (or decay) kinematics due to baryon mean-field potentials on the equilibrium properties of a $N$-$\Delta$-$\pi$ system in a box with periodic conditions. We have found that the inclusion of baryon mean-field potentials in the energy conservation is necessary to maintain the equilibrium state of the $N$-$\Delta$-$\pi$ system, and neglecting this effect would significantly decrease the number of pionlike particles but only slightly decrease the effective charged pion ratio.

We have also used the $\chi$BUU transport model to study pion production in central $^{197}$Au + $^{197}$Au collisions at the incident energy of $E/A = 400$ MeV. It is found that the $\chi$BUU model can well reproduce the experimental measurement by the FOPI Collaboration, thus providing an empirical validation of the behavior of nuclear symmetry energy at high density predicted by the Sk$\chi$m$^*$ energy density functional. We have further predicted the pion kinetic energy dependence of the double and subtract $\pi^-/\pi^+$ ratio as well as the isoscaling pion ratio in central collisions ($b = 3$ fm) of $^{132}$Sn + $^{124}$Sn and $^{108}$Sn + $^{112}$Sn at the incident energy of $E/A = 270$ MeV. Comparing our predictions with future experimental data from the ongoing experiments at RIKEN in Japan by the SPiRIT Collaboration will provide further check on the validity of the Sk$\chi$m$^*$ energy density functional at high density.

## ACKNOWLEDGMENTS

This work was supported in part by the US Department of Energy under Contract No. DE-SC0015266 and the Welch Foundation under Grant No. A-1358.

[1] E. Epelbaum, H.-W. Hammer, and U.-G. Meissner, Rev. Mod. Phys. **81**, 1773 (2009).
[2] R. Machleidt and D. R. Entem, Phys. Rep. **503**, 1 (2011).
[3] B. R. Barrett, P. Navratil, and J. P. Vary, Prog. Part. Nucl. Phys. **69**, 131 (2013).
[4] J. Carlson, S. Gandolfi, F. Pederiva, S. C. Pieper, R. Schiavilla, K. E. Schmidt, and R. B. Wiringa, Rev. Mod. Phys. **87**, 1067 (2015).
[5] G. Hagen, T. Papenbrock, M. Hjorth-Jensen, and D. J. Dean, Rep. Prog. Phys. **77**, 096302 (2014).
[6] H. Hergert, S. K. Bogner, T. D. Morris, A. Schwenk, and K. Tsukiyama, Phys. Rep. **621**, 165 (2016).
[7] Y. Lim and J. W. Holt, Phys. Rev. C **95**, 065805 (2017).
[8] Z. Zhang, Y. Lim, J. W. Holt, and C. M. Ko, Phys. Lett. B **777**, 73 (2018).
[9] R. Navarro Pérez, N. Schunck, A. Dyhdalo, R. J. Furnstahl, and S. K. Bogner, Phys. Rev. C **97**, 054304 (2018).
[10] C. Wellenhofer, J. W. Holt, and N. Kaiser, Phys. Rev. C **92**, 015801 (2015).
[11] C. Wellenhofer, J. W. Holt, and N. Kaiser, Phys. Rev. C **93**, 055802 (2016).
[12] B.-A. Li, Phys. Rev. Lett. **88**, 192701 (2002).
[13] A. W. Steiner, M. Prakash, J. M. Lattimer, and P. J. Ellis, Phys. Rep. **411**, 325 (2005).
[14] J. M. Lattimer and M. Prakash, Phys. Rep. **442**, 109 (2007).
[15] B.-A. Li, C. M. Ko, and W. Bauer, Int. J. Mod. Phys. E **7**, 147 (1998).
[16] B. A. Li, L. W. Chen, and C. M. Ko, Phys. Rep. **464**, 113 (2008).
[17] F. J. Fattoyev, W. G. Newton, and B. A. Li, Eur. Phys. J. A **50**, 45 (2014).
[18] Z. Xiao, B. A. Li, L. W. Chen, G. C. Yong, and M. Zhang, Phys. Rev. Lett. **102**, 062502 (2009).
[19] Z. Q. Feng and G. M. Jin, Phys. Lett. B **683**, 140 (2010).

[20] W. J. Xie, J. Su, L. Zhu, and F. S. Zhang, Phys. Lett. B **718**, 1510 (2013).
[21] J. Xu, C. M. Ko, and Y. Oh, Phys. Rev. C **81**, 024910 (2010).
[22] J. Xu, L. W. Chen, C. M. Ko, B. A. Li, and Y. G. Ma, Phys. Rev. C **87**, 067601 (2013).
[23] M. D. Cozma, Phys. Rev. C **95**, 014601 (2017).
[24] Z. Zhang and C. M. Ko, Phys. Rev. C **95**, 064604 (2017).
[25] B. A. Li, Phys. Rev. C **92**, 034603 (2015).
[26] G. Ferini, M. Colonna, T. Gaitanos, and M. Di Toro, Nucl. Phys. A **762**, 147 (2005).
[27] T. Song and C. M. Ko, Phys. Rev. C **91**, 014901 (2015).
[28] B. A. Li, W. J. Guo, and Z. Shi, Phys. Rev. C **91**, 044601 (2015).
[29] G.-F. Wei, B.-A. Li, J. Xu, and L.-W. Chen, Phys. Rev. C **90**, 014610 (2014).
[30] G.-C. Yong, Phys. Rev. C **96**, 044605 (2017).
[31] M. B. Tsang, J. Estee, H. Setiawan, W. G. Lynch, J. Barney, M. B. Chen, G. Cerizza, P. Danielewicz, J. Hong, P. Morfouace *et al.* (SPiRIT Collaboration), Phys. Rev. C **95**, 044614 (2017).
[32] N. Ikeno, A. Ono, Y. Nara, and A. Ohnishi, Phys. Rev. C **93**, 044612 (2016).
[33] Symmetry energy project https://groups.nscl.msu.edu/hira/sepweb/pages
[34] Y. Zhang, M. B. Tsang, and Z. Li, Phys. Lett. B **749**, 262 (2015).
[35] J. W. Holt, N. Kaiser, G. A. Miller, and W. Weise, Phys. Rev. C **88**, 024614 (2013).
[36] S. Hama, B. C. Clark, E. D. Cooper, H. S. Sherif, and R. L. Mercer, Phys. Rev. C **41**, 2737 (1990).
[37] E. D. Cooper, S. Hama, B. C. Clark, and R. L. Mercer, Phys. Rev. C **47**, 297 (1993).
[38] C. M. Ko, Q. Li, and R.-C. Wang, Phys. Rev. Lett. **59**, 1084 (1987).
[39] C. M. Ko and Q. Li, Phys. Rev. C **37**, 2270 (1988).
[40] G. F. Bertsch and S. Das Gupta, Phys. Rep. **160**, 189 (1988).
[41] S. Huber and J. Aichelin, Nucl. Phys. A **573**, 587 (1994).
[42] Y. Kitazoe, M. Sano, H. Toki, and S. Nagamiya, Phys. Lett. B **166**, 35 (1986).
[43] C.-Y. Wong, Phys. Rev. C **25**, 1460 (1982).
[44] B. Zhang, M. Gyulassy, and Y. Pang, Phys. Rev. C **58**, 1175 (1998).
[45] Z. Zhang and C. M. Ko, Phys. Rev. C **97**, 014610 (2018).
[46] L. Xiong, C. M. Ko, and V. Koch, Phys. Rev. C **47**, 788 (1993).
[47] J. Xu and C. M. Ko, Phys. Lett. B **772**, 290 (2017).
[48] J. Xu, L.-W. Chen, M. B. Tsang, H. Wolter, Y. X. Zhang, J. Aichelin, M. Colona, D. Cozma, P. Danielewicz, Z.-Q. Feng *et al.*, Phys. Rev. C **93**, 044609 (2016).
[49] Y.-X. Zhang, Y. J. Wang, M. Colonna, P. Danielewicz, A. Ono, M. B. Tsang, H. Wolter, J. Xu, L.-W. Chen, D. Cozma *et al.*, Phys. Rev. C **97**, 034625 (2018).
[50] W. Reisdorf, A. Andronic, R. Averbeck, M. L. Benabderrahmane, O. N. Hartmann, N. Herrmann, K. D. Hildenbrand, T. I. Kang, Y. J. Kim, M. Kiš *et al.* (FOPI Collaboration), Nucl. Phys. A **848**, 366 (2010).
[51] G.-C. Yong, B.-A. Li, L.-W. Chen, and W. Zuo, Phys. Rev. C **73**, 034603 (2006).